[1] H. Bethe and R. Peierls, Proc. Roy. Soc. (London) 148A, 146 (1935).

[2] L. Thomas, Phys. Rev. 47, 903 (1935).

[3] G. V. Skorniakov, J. Exptl. Theoret. Phys. (U.S.S.R.) (in press).

[4] M. Verde, Helv. Phys. Acta 22, 339 (1949).

[5] D. G. Hurst and N. Z. Alcock, Canad. J. Phys. 29, 36 (1951).

Translated by R. T. Beyer
171

SOVIET PHYSICS JETP VOLUME 4, NUMBER 5 JUNE, 1957

Measurement of the Ionizing Power of Particles in a Bubble Chamber

G. A. BLINOV, IU. S. KRESTNIKOV AND M. F. LOMANOV

(Submitted to JETP editor June 6,1956)
(J. Exptl. Theoret. Phys. (U.S.S.R.) 31, 762-770 (November, 1956)

The possibility of the measurement of the ionizing power of particles in a propane bubble chamber is demonstrated. The chamber was operating in conjunction with an accelerator. The use of the method of the reduction of pressure to a controllable constant level ensured the stability of chamber operation necessary for ionization measurements. The period of sensitivity was 40 m sec. Measurements of the ionizing power of particles were carried out in the range up to eighty times minimum ionization. It was found that the track density changes with the velocity of the particle as $1/\beta^2$ for $\beta < 0.6$. For velocities close to that of light, relativistic increase in the track density is observed. The used methods on the track evaluation are described.

1. INTRODUCTION

IT was shown by Glaser[1] in 1953 that ionizing particles cause an overheated liquid to boil, leaving tracks in the form of vapor bubble chains. It is possible to describe the expected dependence of the number of bubbles along the track on the charge and the velocity of the particle not entering into the detailed formation mechanism of the nuclei of vaporization under the influence of ionization. It is well known that an overheated liquid starts boiling on the vaporization nuclei, the radius of which is greater than a critical value r_{cr}.

$$r_{cr} = 2\sigma/(P_\infty - P_0), \qquad (1)$$

where σ is the surface tension coefficient of the liquid-vapor boundary, P_∞ is the pressure of the saturated vapor and P_0 is the hydrostatic pressure of the liquid. The energy losses of a particle due to the ionization of the medium can entail conditions favoring the formation of vaporization nuclei. Bubble chambers usually operate at values of σ in the range from 1–10 dyne/cm and of $(P_\infty - P_0)$ in the range from 5 to 20 atm, which correspond to $r_{cr} = 10^{-5} - 10^{-6}$ cm.

It is evident that the nuclei of vaporization are formed in the region where the ionization density, over distances of the order of r_{cr} is considerably larger than the average ionization density along the particle trajectory. This condition is fulfilled by the end points of the tracks of the δ-electrons produced by the particles. Indeed, electrons of about 200 ev lose all their energy on a path shorter than 10^{-5} cm in a liquid, producing some 20 ion pairs*, while for the case of a relativistic particle, the number of ion pairs along the trajectory is not greater than 0.5 per 10^{-5} cm, and the probability of many acts of primary ionization over such a length is vanishingly small. It can be therefore assumed that the number of bubbles along the path of the particle is proportional to the number of δ-electrons of energy greater than 100–200 ev. Neglecting the binding energy of electrons in the atom, we shall obtain the following expression for the number of bubbles per unit length of track (track density):

$$g = g_0 Z^2/\beta^2, \qquad (2)$$

where g is the track density, Z is the charge of the particle, β is the particle velocity in terms of the velocity of light, and g_0 is a coefficient depending on the stopping power of the medium, on the temperature and on the "overheating" $P_\infty - P_0$.

*The given values of range and of the number of ion pairs are calculated for the case of liquid propane from data concerning the air.[2]

For $\beta \approx 1$, relativistic corrections taking into account the polarization of medium should be introduced into Eq. (2).

Authors of various experimental investigations[3-7] have not noted that a difference is observed in the density of tracks belonging to different particles; the correlation, however, of the track density with the velocity of the particle has not been found, due to a number of difficulties. In contrast with other authors, who used a constant chamber expansion, we applied the method of pressure reduction to a certain level, which ensured the high stability of the chamber operation necessary for such correlation.

The experimental work was carried out with the synchrocyclotron of the Institute for Nuclear Problems of the Academy of Sciences USSR.

2. CHAMBER CONSTRUCTION AND CHOICE OF OPERATING CONDITIONS

The working volume of the chamber (A, Fig. 1) consists of a cylindrical vessel of stainless steel of 92 mm internal diameter and 70 mm high, the ends of which are covered by glass plates 30 mm thick. The joint is made tight by a 1 mm thick fluoroplast gasket. The liquid used is singly distilled technical grade propane, with the vapor pressure equal to 30 atm at 64° C. Water for heating the chamber flows from a thermostat through the pipes 1 and 2 to the chamber and circulates in channels between the chamber's body and its covers. The chamber temperature was usually equal to 64° C with stability better than 0.1° C.

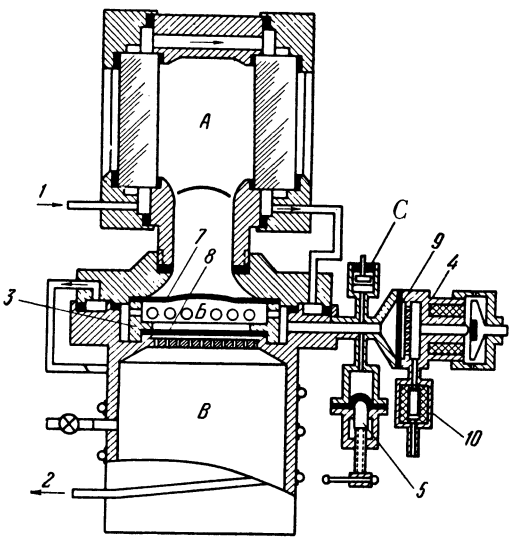

FIG. 1. Chamber construction (schematic).

The volume B, filled with water, is connected through openings in the gasket ring 3 with the electromagnetic exhaust valve 4, the vapor phase volume control 5 and the capacitance pressure gauge 6. The working volume of the chamber is separated from the volume C by a fluoroplast diaphragm 7. As long as the external pressure is not supplied (the valve 4 is open), the diaphragm 7 remains in the intermediate position, and the rubber diaphragms 8 and 9 are pressed against the respective grids. The vapor phase then has a volume equal to 16 cm.^{3} Since the total volume occupied by the propane equalled 660 cm^3, the maximum volume expansion coefficient amounted to 16/660 = 0.024. The expansion coefficient could be varied by means of the control 5, consisting of a piston with a rubber diaphragm.

The peculiarity of the operation of the chamber lies in the reducing of the pressure to a constant controllable level. The level is set by the pressure of the carbon dioxide gas, which fills the volume B.

The operation of the chamber is as follows: carbon dioxide at 38 atm is supplied to the rubber diaphragm 9 through a pressure stabilizer (not shown in the drawing) and the electromagnetic inlet valve 10. This pressure is transmitted by the water to diaphragms 7 and 8, the diaphragm 8 moving against the grid, while the diaphragm 7 compresses the propane. The vapor phase in the chamber condenses completely, and the chamber is ready for expansion.

The moment of expansion is chosen by means of a radio frequency control, the antenna of which is placed near the synchrocyclotron chamber. The antenna is sharply tuned to a frequency close to that of particle ejection. Out of a train of amplified and shaped pulses one is selected, which, after a controllable delay, causes the exhaust valve 4 to open. Within 12 m sec the chamber pressure falls to the value equal to the pressure in the volume B. The delay between the synchronizing signal and the beginning of the pressure reduction is chosen so that particles of one of the consecutive intensity pulses traverse the chamber at the stationary pressure P_0. The schematic time diagram of chamber operation, obtained by means of the capacitance gauge and an oscilloscope, is shown in Fig. 2.

Two pulsed illumination lamps of the type ISS 250 were switched on after the passage of the particles. The chamber is flooded by light aimed towards the camera at an angle of 30° to the camera aiis in order to prevent the incident beam from striking the lenses. Dark background is used for

the photography. A stereocamera with 75 mm lenses at an aperture of $f/60$ and a reduction of 3.5 diameters is used. The light flash duration is 1 to 4 m sec. the exact time within these limits being chosen to produce the best images of the smallest bubbles. About ten seconds are needed for preparing the chamber for the next expansion.

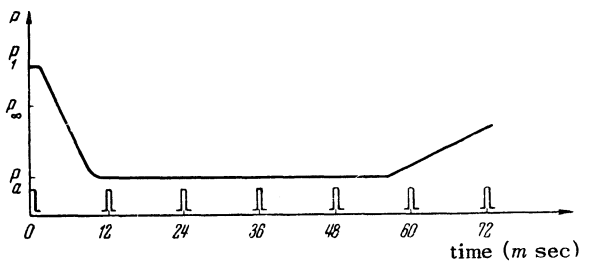

FIG. 2. Change of the pressure in chamber during expansion. $P_1 = 38$ atm, $p_\infty = 30$ atm— pressure of the saturated vapor of the working liquid at 64° C; P_0 — level of the pressure reduction (22–25 atm). Times of the passage of particles from the accelerator are shown. Duration of pulse about 300 μ sec.

In the first variant of the chamber, the working volume was connected with the volume C by a pipe of 12 mm internal diameter. A fast reduction of pressure caused a turbulent ebullition in this pipe which considerably shortened the sensitivity period of the chamber. The pipe diameter was therefore enlarged to 50 mm. This resulted in a period of sensitivity in excess of 40 m sec, which was tested by photographing particle tracks from three intensity pulses of the accelerator. The measurements of the track density of fast electrons have shown that the chamber sensitivity varies by a factor of about 1.5 from one intensity pulse to the next, arriving 12 m sec later. Synchronization of the beginning of the pressure reduction with the accelerator pulses made it possible, however, to obtain consistently reproducible results. Measurements have shown that the sensitivity is uniform over the whole volume of the chamber, and is constant for hundreds of pictures taken under the same operational conditions.

The sensitivity of the chamber could easily and quickly be controlled by the gas pressure in the volume B. This method was used for the selection of the sensitivity at which ionization measurements in the given region were most accurate. The resulting dependence of the sensitivity of the chamber on the "overheating" $P_\infty - P_0$ at the temperature of 64° C is given in Fig. 3. It can be seen that it is necessary to keep the pressure P_0 constant within a few hundredths of an atmosphere in order to ensure the stability of the operation of the chamber. In our case, this was effected by hermetic sealing of the volume B (Fig. 1) containing the gas, and the thermostating of it together with the body of the chamber.

In the course of the work with the accelerator, the chamber was placed either into the emerging collimated neutron beam with a mean energy of 590 mev, or into the beam of γ-rays from the π^0-meson decay, or into the beam of particles emitted from the targets and the walls of the collimator in the direction of the proton beam. The control system governing the necessary synchronization and delay was placed at a considerable distance from the chamber behind a concrete shield. This system also permitted remote measurement of the temperature and pressure in the chamber, and the remote control of the motor, the thermostat heaters, the light flashes, and the pressure. At a dangerously high pressure the thermostat was automatically switched off and the exhaust valve opened, preventing the chamber from exploding.

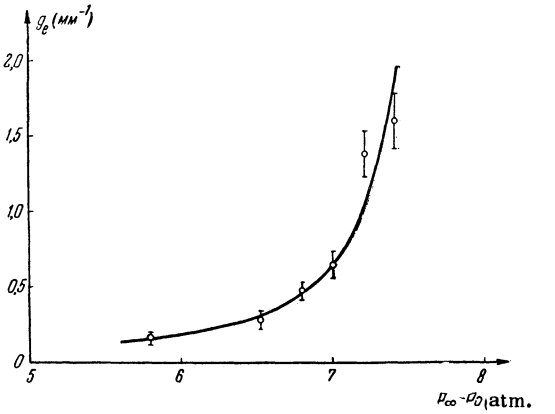

FIG. 3. Dependence of the track density of minimum ionization electrons (E = 1–5 mev) on the "overheating" ($P\infty - P_0$) for P = 30 atm.

3. METHODS OF TRACK DENSITY MEASUREMENTS

The observed number of bubbles usually differs from the number of primarily produced bubbles. There are several causes of this: overlapping of the bubble images, interaction of closely spaced growing bubbles and subjective errors on the part of the observer connected with the difficulty of discerning single bubbles in clusters. At present, the methods of the measurement of the mean gap length and of the number of gaps are used for the determination of the track density in nuclear emulsions; these exclude the sources of the above errors. Analogous methods were used by us. Formulas correlating the measured value with the

track density depend on the statistical distributions of bubbles along the track. In accordance with our ideas about the bubble creation mechanism mentioned in the introduction, the bubbles, similarly to δ-electrons, should be produced with equal probability at any point of the path of the particle, provided its velocity is constant. In this case the probability of finding n bubbles on the length x is given by the Poisson distribution:

$$w(n, gx) = (gx)^n e^{-gx}/n!, \qquad (3)$$

where g is the track density.

Comparison with experiment revealed marked deviation from the Poisson distribution for tracks consisting of bubbles of a relatively large diameter (< 0.2 mm) and an observed density of more than two bubbles per mm (Fig. 4*b*). Such tracks appear sometimes as uniform chains of bubbles, the number of bubbles being largely independent of the velocity of the particle. This effect is caused by the interaction of the neighboring bubbles during their increase. Further measurements were therefore made only for the case of tracks consisting of sufficiently small bubbles, so that their optical images were essentially smaller than the developed images on the film. The effects connected with bubble interaction are then negligible. The preponderant majority of the pictures obtained conformed with this condition. The average diameter of the bubble image on the film was 0.035 mm, which, taking into account the camera reduction, gives 0.1 mm, while the real bubble was approximately half this size. The distribution obtained for such tracks is shown in Fig. 4*a*. The slight narrowing of this distribution, as compared to Poisson distribution, is explained by the overlapping of bubble images.[8]

Tracks of various densities were treated by different methods depending on the measure of the overlapping of the images gD, where D is the mean diameter of the bubble image, the camera reduction factor being accounted for. The three methods of track density measurement described below were chosen as the most sensitive.

1. The method of the straightforward bubble counting, or, more exactly, of the measurement of the length of the blackened part of the track, was used for $gD < 0.4$. It can be shown that, in this case, the track density is given by the following expression:

$$g = \frac{1}{D} \ln \frac{1}{1 - (L'/L)}, \qquad (4)$$

where L' is the length of the blackened part of the track, and L is the total track length.

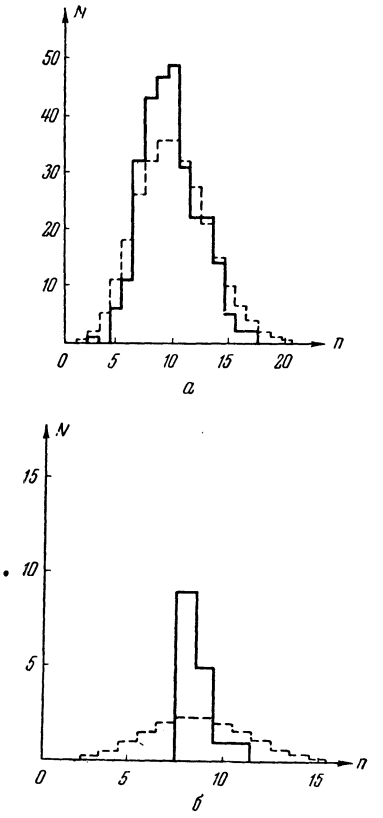

FIG. 4. Distribution of the cases of the production of n bubbles on a length x of the tracks for monoenergetic particles. *a*— "good" tracks; interaction of neighboring bubbles not visible in photographs. Bubble diameter less than 0.05 mm, diameter of the bubble image (camera reduction accounted for) $D = 0.1$ mm, $g = 3$ mm^{-1}, $x = 3.5$ mm. *b*—"bad" tracks, diameter of bubbles equal to image diameter, D—0.5 mm; observed track density $g_{obs} = 2$ mm^{-1}, $x = 4$ mm, broken line represents the Poisson distribution.

In practice, the length of the blackened part was determined by counting the number of bubbles under the assumption that the number of bubbles in a cluster equals the length of the cluster divided by the diameter of a single bubble. The length of a cluster was estimated visually, which entailed subjective errors. For small values of overlapping ($gD < 0.4$), however, the subjective error is small and the method was widely used because of its simplicity. In this case, Eq. (4) has the following form, obtained by Williams[9]:

$$g = \frac{1}{D} \ln \frac{1}{1 - kD}, \qquad (5)$$

where $k = N/L$ and N is the observed number of bubbles. The statistical error is given by the formula:

$$\Delta g/g = N^{-1/2}. \qquad (6)$$

2. The mean gap length method is the most objective one, since its results do not depend on the average bubble diameter. It is more difficult than the first method.

It is known[10] that the gap length distribution is exponential:

$$W(l)\,dl = ge^{-gl}dl, \qquad (7)$$

where $W(l)\,dl$ is the probability of the gap length to fall between l and $l \neq dl$. This fact is confirmed by direct measurements of fast electron tracks (Fig. 5). It can be seen from the histogram, however, that the experimental distribution differs from the theoretical only for gap lengths smaller than $D/2$. This is connected with the fact that the outlines of the bubble images are blurred. The method of the measurement of the mean length of gaps larger than a certain value ϵ was therefore used. ϵ was usually taken to be equal to $D/2$.

The track density can be found from the measured mean gap length larger than ϵ according to the following formula:[10]

$$g = 1/(l_\varepsilon - \varepsilon) \qquad (8)$$

with a statistical error

$$\Delta g/g = N_\varepsilon^{-1/2}, \qquad (9)$$

where N_ϵ is the number of such gaps, and l_ϵ their mean length.

3. For dense tracks ($gD > 1$), the method of counting of the number of gaps larger than ϵ is more accurate. According to reference 10, the number of tracks is connected with the track density by the following relation:

$$N_\varepsilon = gLe^{-g(D+\varepsilon)}. \qquad (10)$$

The dispersion of the gap number distribution in an analogous problem was calculated by Domb[11]: Making use of his results, the statistical error of the track density is easily found to be:

$$\frac{\Delta g}{g} = \frac{(1 - 2j_\varepsilon e^{-j_\varepsilon})^{1/2}}{\sqrt{N_\varepsilon}\,|1 - j_\varepsilon|}, \qquad (11)$$

where

$$j_\varepsilon = g(D + \varepsilon).$$

The validity of the formulas for the statistical error estimate was checked by us experimentally. Some 23 fast electron tracks were used for this purpose. The tracks were divided into intervals of equal length, and the dispersion of the distribution of the values of N, N_ϵ and l_ϵ was measured. The result of the measurements can be represented in the following form:

$$\Delta g/g = C/\sqrt{N_m}. \qquad (12)$$

where N_m is the number of counts of bubbles or gaps larger than ϵ. The coefficient C depends on the method used and on the value of $j_\epsilon = g(D + \epsilon)$.

The theoretical dependence of C on j_ϵ for the different methods and the experimental points are shown in Fig. 6. The satisfactory agreement between the experimental points and the theoretical curve indicates the correctness of the application of the formulas (6), (9) and (11) for the calculation of statistical errors.

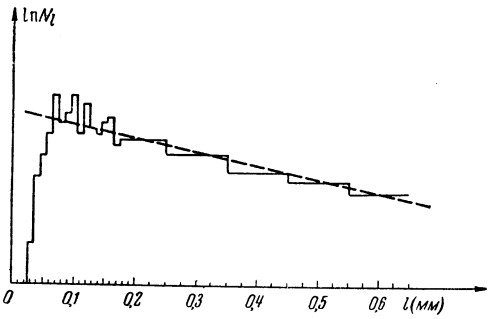

FIG. 5. Gap length distribution. N_l —number of gaps with length between l and $l + dl$.

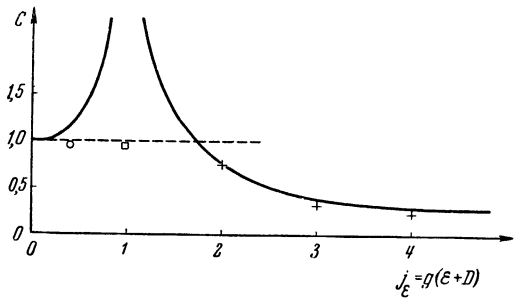

FIG. 6. Dependence of coefficient C in Eq. (12) on $j_\epsilon = g(D + \epsilon)$ +—gap number method (solid curve); ☐—mean gap length method (broken line); O—straightforward bubble counting.

It was assumed in the calculations that all the bubble images are of the same diameter. In reality, the values are distributed. with an average value equal to D (taking the camera reduction into account) and a dispersion σ^2. In our case, the ratio σ/D equalled 0.1, and the distribution width

was negligible. It is desirable to have a smaller D for better accuracy. The ratio σ/D is then larger. It was found from cloud chamber pictures, taken by 3. V. Chirokov, that $\sigma/D = 0.4$ for $D = 0.05$ mm. The results of measurements of the statistical error for tracks 5 cm in length, depending on the measure of overlapping, are given in the Table for two values of the ratio σ/D. The errors are given for the most accurate method of measurement in each case.

It can be seen from the Table that, for tracks 5 cm in length, the variation of the density by a factor of 20 with an error of 6–10% is possible without any change of the chamber sensitivity setting.

By controlling the chamber sensitivity and using various methods of track density measurements we measured ionization, varying from minimum ionization up to a value greater by a factor of eighty.

	Method of Measurement	number of bubbles	mean gap length $\epsilon = D/2$	number of gaps $\epsilon = D$	number of gaps $\epsilon = D/2$
$\Delta g/g(\%)$	gD	0,2 0,3	0,4 0,8	0,9 1,2	1,4 2,0 3,0 4,0
	$D = 0{,}1$ мм $\sigma/D \leqslant 0{,}1$	10,5 8,8	9,5 9,0	9,2 7,3	6,7 6,3 6,7 9,0
	$D = 0{,}05$ мм $\sigma/D = 0{,}4$	8,8 7,7	8,1 7,5	7,5 6,1	5,9 5,7 7,0 10

4. IDENTIFICATION OF PARTICLES AND DEPENDENCE OF THE TRACK DENSITY ON PARTICLE VELOCITY

Since the particle beams used by us were not monoenergetic, correct identification of the particles from their tracks constituted a most important problem.

The stopping power of the liquid used was determined from the range of monoenergetic muons from the $\pi-\mu$ decay (Fig. 7) obtained by means of the proton beam. The measured mean range of four muons equalled 3.05 ±0.12 mm, which agrees with the value calculated for propane at muon energy of 4.17 mev. The photographs obtained with the neutron beam contained a large number of tracks of different particles. The horizontal tracks of stopping ionizing particles and tracks of electrons of various energies were selected for evaluation.

The identification of the particle tracks was done in the following way: particles having minimum ionization tracks with strong multiple scattering were classified as electrons (Fig. 8), which were in turn divided into two energy groups. Tracks with strong multiple scattering, terminating in the chamber, correspond to electrons of energy between 1 and 5 mev, and tracks with weaker scattering, extending beyond the chamber, to electrons of 10–100 mev. Protons, deuterons and pions stopping in the chamber were identified on the basis of a number of criteria: 1) the total number of bubbles in a chosen residual range 2) the dependence of track density on range 3) the value of the multiple scattering and 4) the nuclear interaction at the end of the pion track (Fig. 9).

The distribution of the total number of bubbles over the residual range equal to 36 mm for 20 stopping particles is shown in Fig. 10. The corresponding photographs were obtained at low sensitivity conditions, where the tracks of fast electrons had a density of 0.24 bubbles per mm and were almost invisible (operation conditions No. 1, $P_0 = 24.2$ atm). As it can be seen from the histogram, the tracks are divided into three groups with the mean values of 51,100 and 131 bubbles in the residual range of 36 mm. According to the criteria given above, the particles of the first group were identified as pions, of the second as protons, and of the third as deuterons. These particles leave the steel walls of the chamber, and also are formed within the chamber during the disintegrations of nuclei by neutrons. On the basis of conservation law considerations and the initial energy of the neutrons it was shown that α-particles cannot be found among particles having a residual range of 36 mm in propane, and the proportion of tritium nuclei cannot be significant because of their low frequency in stars.[12]

The width of each group is well explained by the statistical spread of the number of bubbles. It is also easily shown that the probability of the fluctuation by which a particle from the second group can be found in the third group is smaller than 1%.

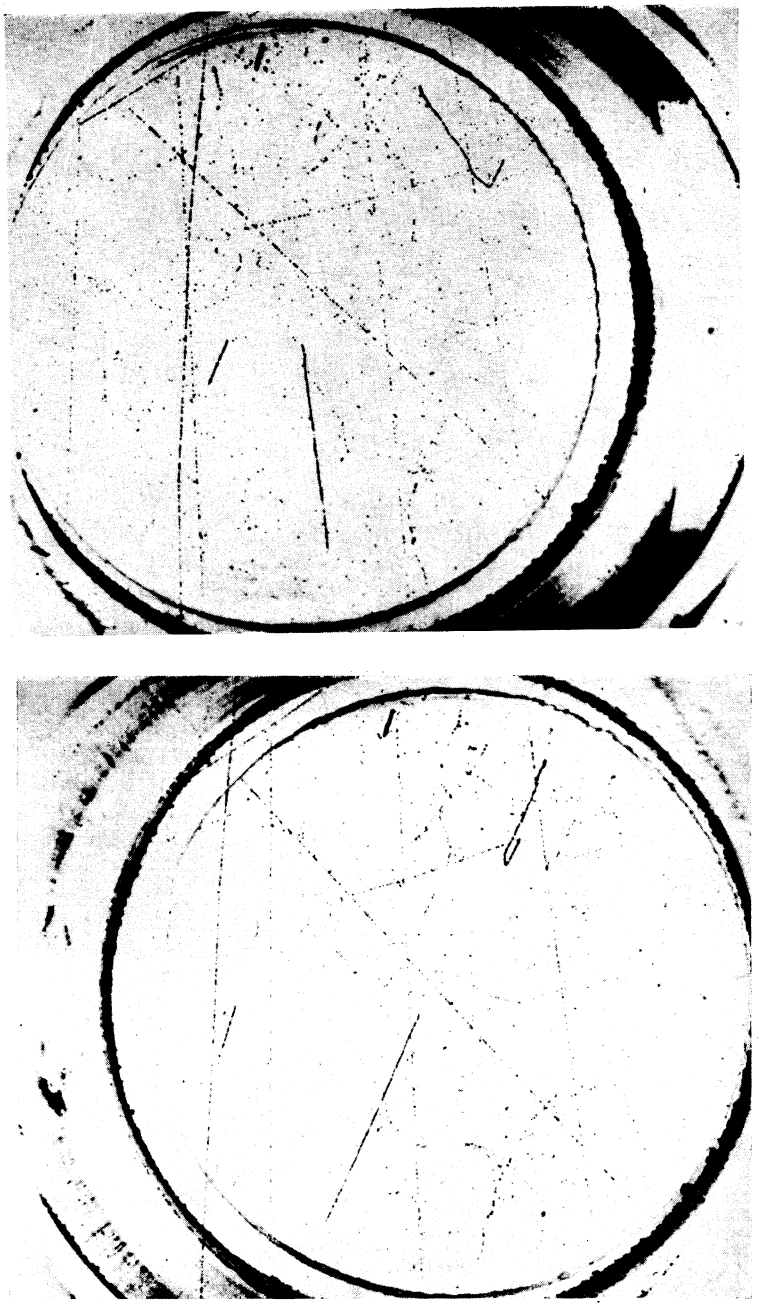

FIG. 7. Photograph of π–μ–e decay. The pion emerges from the rear window of the chamber.

The measurements showed that the track density varied approximately as $1/\beta^2$, β being determined from the range and the assumed mass of the particle. The measured ratios of the numbers of bubbles

$$N_p / N_\pi = 1.96 \pm 0.25 \text{ and } N_d / N_p = 1.31 \pm 0,08$$

are in good agreement with the ratios calculated under the assumption of a $1/\beta^2$ dependence:

$$(N_p/N_\pi)_{\text{calc}} = 2.2; \qquad (N_d/N_p)_{\text{calc}} = 1.35.$$

For more accurate results, the tracks were divided into intervals of 3 mm each, and the mean track density was determined in intervals with a given distance to the end of the track for every

particle group. Tne velocity was determined from the range and the mass of the particle. The dependence of the track density on the velocity of particle was sought inthe form

$$g = g_0/\beta^n. \quad (13)$$

The values of g_0 and n, found with the help of the least squares method for operation conditions *I*, are: $n = 2.07 \pm 0.17$; $g_0 = 0.155$ mm^{-1}.

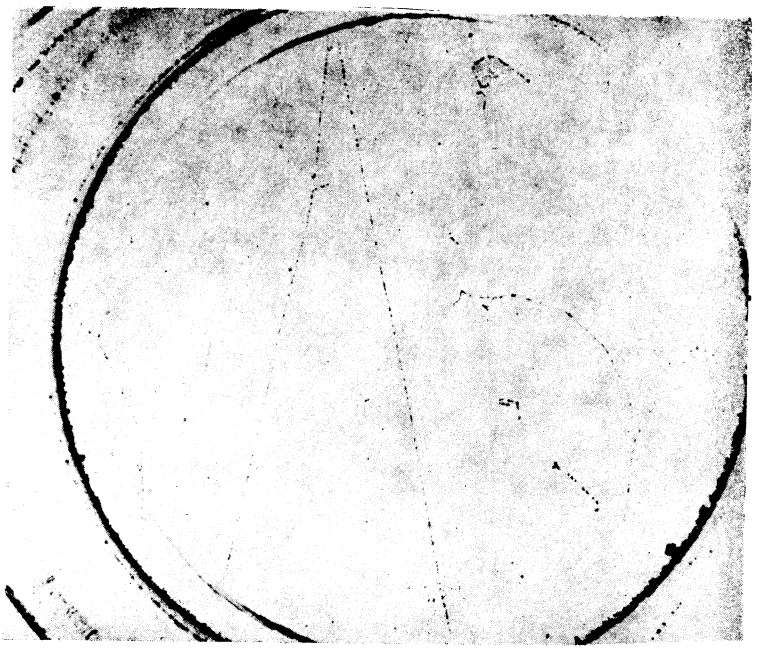

FIG. 8. Tracks of electrons of various energies. The electrons are produced inthe walls ofthe chamber, placed in a beam of γ-rays.

For higher sensitivity of the chamber (operation conditions *II* $P_0 = 23.5$ atm) the analysis of 7 cases of protons, 2 deuterons and 7 electrons yielded the following values: $n = 2.02 \pm 0.34$; $g_0 = 0.200$ mm^{-1}.

For operation conditions *III* ($P_0 = 22.8$ atm, $g_0 = 0.28$), tracks of four pions and 29 electrons were analyzed, one of the pions, which left the chamber, being identified by multiple scattering. The value of n was not determined since the number of particles coming to a stop was small, while g_0 was obtained from the comparison of the electron track densities with those of operation conditions *II*.

The experimental data on the dependence of the track density on the particle velocity for all three operation conditions are shown in Fig. 11. It was assumed that $n = 2$ and new values of g_0 were calculated. The straight line in Fig. 11 corresponds to the equation

$$g/g_0 = 1/\beta^2. \quad (14)$$

Satisfactory agreement of the experimental points for all three operation conditions with Eq. (14) permits us to conclude that the value of g/g_0 is directly related to the velocity of the particle or, more accurately, to the ratio Z^2/β^2. An increase in the track density, deviating from Eq. (14), is observed for electrons of velocities close to the velocity of light. Measurements of 148 cases have shown that tracks of electrons of 10–100 mev have a density 12 5% higher than the tracks of 1–5 mev electrons.

It is possible to state, therefore, that a relativistic increase ofthe track density exists in the bubble chamber.

The authors wish to express their gratitude to A. I. Alikhanov, A. G. Meshkovskii and 3. V. Chirikov for discussion of results and to M. G. Meshcheriakov for making it possible to use the synchrocyclotron of the Institute of Nuclear Problems.

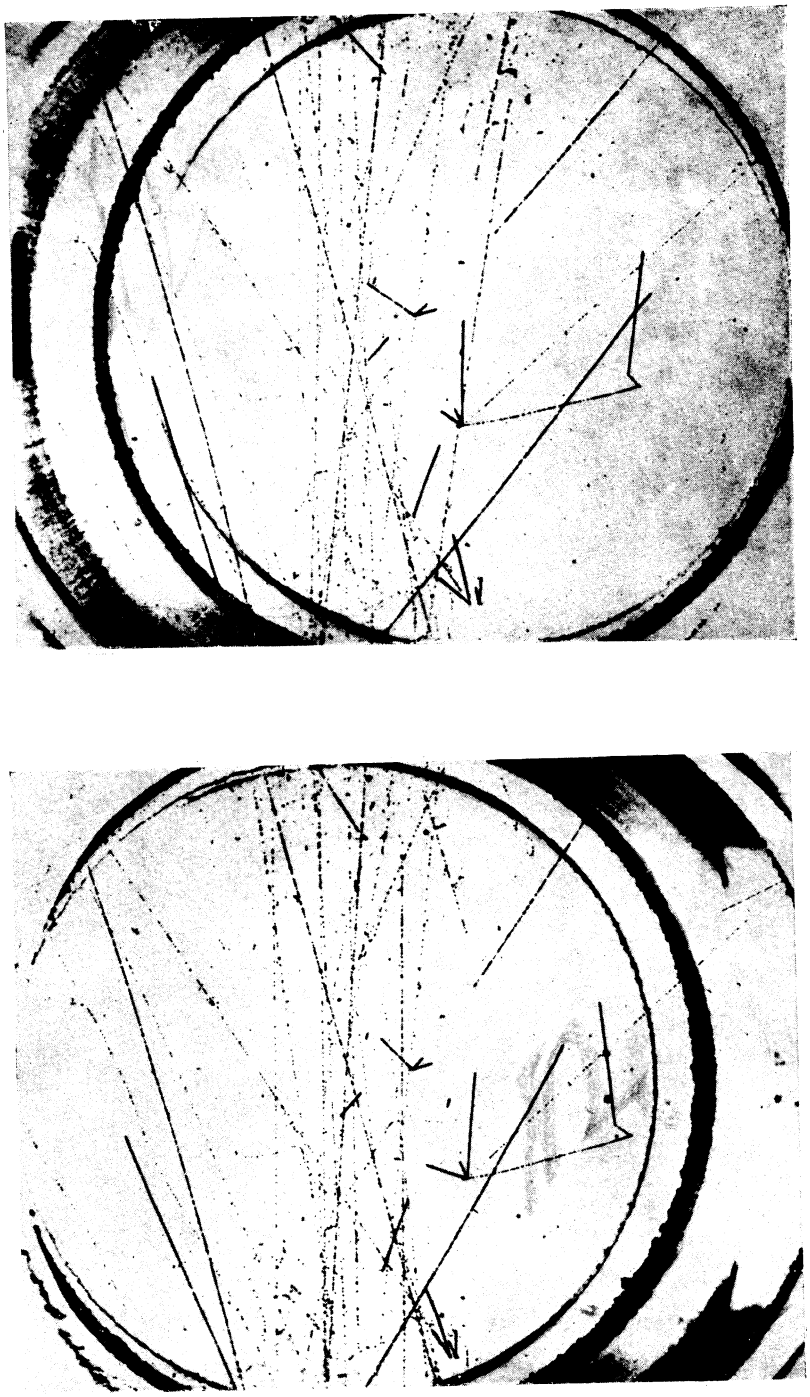

FIG. 9. Pion stopping in the chamber produce a two-prong star. The pion was created in disintegration of a C nucleus by a neutron (six-prong star). Tracks of protons and electrons produced by the neutron beam which traverses the chamber (mean energy 590 mev) are also visible in the photograph.

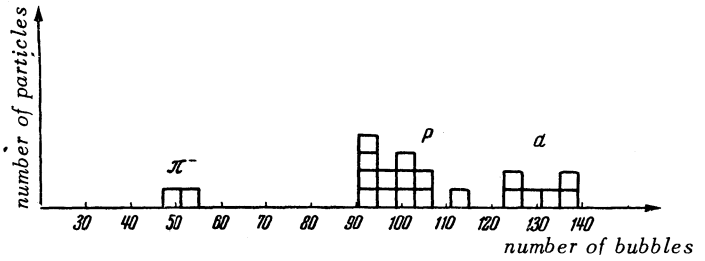

FIG. 10. Distribution of the number of bubbles in the residual range of 36 mm in tracks of stopping ionizing Particles.

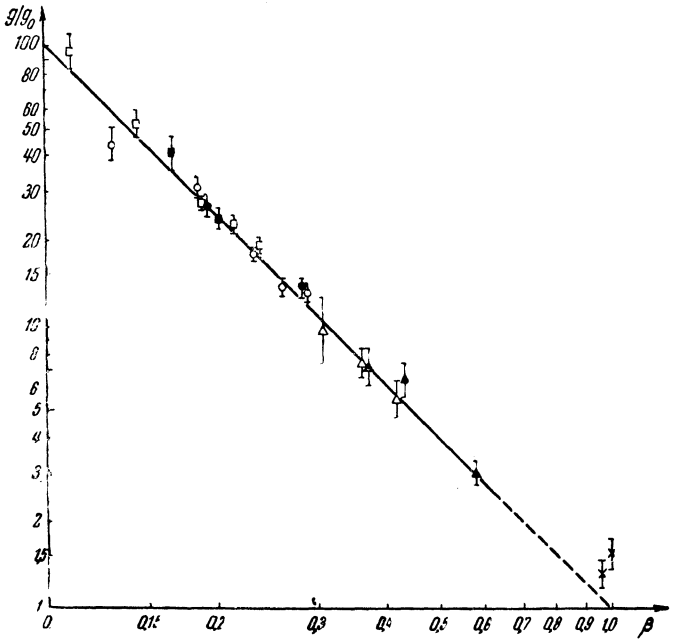

FIG. 11. Dependence of g/g_0 on β. Log–Log coordinates. O–protons, □ –deuterons and Δ–pions for operation conditions *I*; ●–protons, ■–deuterons and X–electrons for conditions *II*; ▲–pions and X–electrons for conditions *III*.

[1] D. A. Glaser, Phys. Rev. **91**, 762 (1953).

[2] Landolt-Bornstein, Zahlenwerte und Funktionen, 6 Auflage, 1952, I Band, 5 Teil, S. 343.

[3] D. A. Glaser and D. C. Rohm, Phys. Rev. **97**, 474 (1955).

[4] Blinov, Krestnikov and Pershin, Dokl. Akad. Nauk SSSR **99**, 929 (1954).

[5] Blinov, Krestnikov and Pershin, Izv. Akad. Nauk SSSR, Ser. Fiz. **19**, 758 (1955).

[6] C. Dodd, Nature **176**, 142 (1955).

[7] D. Parmentier and A. J. Schwemin, Rev. Scient. Instr. **26**, 954 (1955).

[8] Happ, Hull and Morris, Canad. J. Phys. **30**, 699 (1952).

[9] E. J. Williams, Proc. Roy. Soc. (London) **A172**, 207 (1939).

[10] M. G. K. Menon and C. O.'Callaigh, Proc. Roy. Soc. **A221**, 292 (1954).

[11] C. Domb, Proc. Camb. Phil. Soc. **43**, 329 (1947).

[12] Bernardini, Booth and Lindenbaum, Phys. Rev. **85**, 826 (1952).

Translated by H. Kasha
169